

# Parameters Based AE Analysis



Dimitrios G. Aggelis and Tomoki Shiotani

**Abstract** The present chapter discusses the parameter-based analysis of AE. This is particularly useful in case full waveform recording is not available, or the acquisition rate is not sufficient to allow waveform streaming. Parameter analysis is based on extraction of descriptors that contain most of the waveform information, without however, the need to store the whole number of points, essentially contributing to data management. The different parameters are introduced and their relation to fracture mode as well as their use for process characterization are discussed in detail. In addition, well established indices based on the total AE activity are also discussed to demonstrate the complete arsenal of AE parametric analysis that has proven very useful to researchers and practitioners, in different material systems.

**Keywords** Frequency · Rise time · RA-value · Duration · Fracture mode · Matrix crack · Fiber rupture · Delamination · Tension · Shear · Kaiser effect · Calm ratio

## 1 Basic Experimental Details and Parameters

The final goal of monitoring AE phenomena is to provide beneficial information to prevent fatal failure by correlating the detected AE signals with the ongoing fracture process or deterioration of a material or structure. AE activity is observed transiently or continuously, and the signals generally contain frequency components over the audible range as well as a variety of durations.

The AE technique detects and monitors the transient elastic waves that are emitted after an irreversible phenomenon or process in the material. In most cases, piezoelectric transducers are placed on the surface of the material under test. The sensors

---

D. G. Aggelis (✉)

Department of Mechanics of Materials and Constructions, Vrije Universiteit Brussel, Brussels 1050, Belgium  
e-mail: [Dimitrios.aggelis@vub.be](mailto:Dimitrios.aggelis@vub.be)

T. Shiotani

Department of Civil and Earth Resources Engineering, Graduate School of Engineering, Kyoto University, C-Cluster, Katsura Campus, Kyoto University, Kyoto 615-8540, Japan  
e-mail: [shiotani.tomoki.2v@kyoto-u.ac.jp](mailto:shiotani.tomoki.2v@kyoto-u.ac.jp)

© Springer Nature Switzerland AG 2022

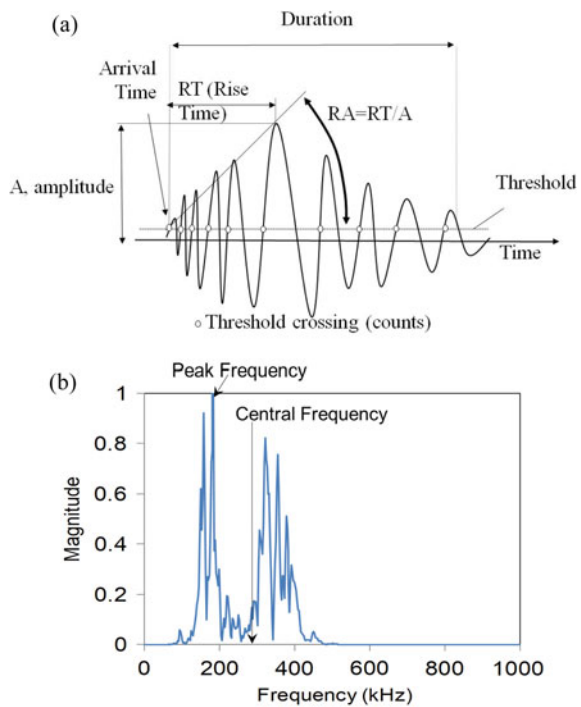
C. U. Grosse et al. (eds.), *Acoustic Emission Testing*, Springer Tracts in Civil Engineering, [https://doi.org/10.1007/978-3-030-67936-1\\_4](https://doi.org/10.1007/978-3-030-67936-1_4)

transform the pressure on their surface into electric waveforms. These waveforms are pre-amplified and are led to the digitization and acquisition board. Apart from recording the full waveform which is always an option in most contemporary systems, the basic parameters of each waveform are measured and stored as well.

The total activity of AE (simply how many “hits” are recorded by any sensor) is indicative of the phenomenon under monitoring. In case this phenomenon is fracture, the number of hits is related to the damage degree and the rate of crack formation and propagation. In addition, the shape of the waveform yields important information relatively to the source of the emission. The early AE systems, not having the capacity for recording full waveforms of thousands of points, extracted only a set of features indicative of the waveform shape which were also powerful for source characterization. Therefore, many parameters are used for the quantification of the waveform. The basic ones are shown in Fig. 1 and are explained below.

- **Threshold:** A predefined voltage that must be overpassed by the incoming waveform in order to trigger the acquisition. It also helps to avoid low amplitude noise signals.
- **Hit:** a signal that exceeds the threshold and causes a system channel to record data.

**Fig. 1** A typical AE waveform with main parameters in **a** time domain, and **b** frequency domain



- **Threshold crossings (Counts):** the number of times within the signal, where the threshold is exceeded (in Fig. 1a, this number is 10). Like almost all AE parameters, counts strongly depend on the level of the applied threshold. Counts between the onset (1st count) and the peak amplitude is referred to as “Counts to Peak”. Similarly, someone can use “Counts to decay”, where obviously the sum of the last two descriptors is equal to the total “Counts”.
- **Amplitude, A:** The peak voltage of the signal waveform (positive or negative). Amplitudes are expressed on a decibel scale instead of linear scale where usually 1  $\mu\text{V}$  at the sensor is defined as 0 dB AE. The amplitude is closely related to the magnitude of the source event but as the propagation distance increases, the attenuation will strongly compromise the final amplitude value at the sensor. This parameter is typically used to determine the system’s detectability.
- **Duration, DUR:** the time interval between the 1st count and the last descending threshold crossing. The duration is generally expressed in  $\mu\text{s}$  (microseconds) and is connected to the source magnitude and type.
- **Rise Time, RT:** the time interval between the triggering time of AE signal (1st count) and the time of the peak amplitude. The rise time is closely related to the source-time function and is applied to classify the type of fracture. Similarly, to the counts to decay, one can use “decay time”, where the sum of rise- and decay-time is equal to the duration.
- **Energy, ENE:** definitions of energies are different in AE system suppliers, but it is generally defined as a measured area under the rectified signal envelope (MARSE). The term “signal strength” is also found under the same definition. The energy is preferred to interpret the magnitude of source event over counts because it is sensitive both to the amplitude and the duration, and less dependent on the voltage threshold and operating frequencies. While this is an “engineering” value, another definition of energy, namely “absolute energy” comes from the integration of the rectified waveform envelope squared, is measured in “attoJ” and is considered analogous to the actual energy freed from the source:

$$E_{\text{abs}} = \int_0^{t_1} V^2(t) dt \quad (1)$$

where the waveform starts at time 0 and ends at  $t_1$ .

The frequency content is also essential. Different parameters are used for the process of this field of information. The simplest is the:

- **Average Frequency, AF,** which is calculated in time domain as the ratio of the total number of counts over the duration of the waveform in kHz. Currently, with the rapid progress of computer technology, AE waveforms can be recorded readily as well as the parametric features. Thus, waveform-based features as peak frequency (PF) and frequency centroid or central frequency (CF) are additionally determined in real time from the fast Fourier transform (FFT) of recorded waveforms. AE parametric features are thus extracted and provide useful information to correlate with the failure behavior of materials. The first (PF) is the frequency with the

highest magnitude in the FFT and the latter (CF) is the centroid of the FFT (see Fig. 3b), which is given by:

$$CF = \frac{\int_0^f fH(f)df}{\int_0^f H(f)df} \quad (2)$$

where  $f$  is the frequency, and  $H(f)$  the magnitude of the FFT.

Practically, the early part of the waveform contains information more relevant to the source mechanism, while the latter part may contain reflections and possibly the “ringing effect” of the (resonant) sensor. Parameters like the RT, Duration, RA exhibit high values for fracture sources of shear character while they show low values for tensile fracture as will be discussed in detail below.

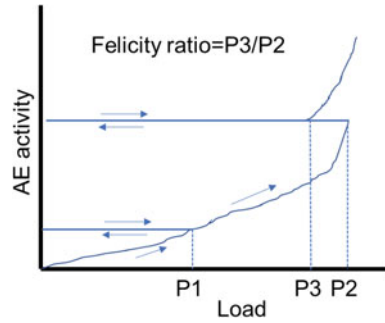
Based on the shape of the first part of the waveform the ‘RA value’ has been introduced which is defined by RT over A and is the inverse of the opening “slope” of the waveform [1] (see Fig. 1a). The slope is called “Grade” in older studies [2, 3]. RA is measured in  $\mu\text{s/V}$ , being increasingly used for the fracture mode determination in different material fields.

The way that data are treated after the AE acquisition depends on the application, the setup and the preference of the user. Different approaches can be used with success. Some are based on the total AE activity relatively to the active load or developing damage. Others use the amplitude and its statistical distribution, while others utilize the parameters of waveforms with the aid of simple or more complex tools (pattern recognition) to exploit the hidden information. Details about these approaches are given in the following subsections. Treatment of full waveforms (as in “signal-based” analysis, which is covered in Chap. “Signal-Based AE Analysis” of the book) is also very widely used.

## 2 Basic AE Indices and Correlation with Material Condition

One of the most basic phenomena in the field of AE is the so called “Kaiser” effect [4]. It received its name by Dr. Joseph Kaiser who was one of the pioneers of the modern AE technology. During the increase of the mechanical load in a specimen (metal in the original study), it is normal to record acoustic activity due to possible development of micro-cracking (moderate load P1 in Fig. 2). In case of unloading and reloading, no AE is observed (at the same sensitivity level or with the same threshold) until the previous maximum load P1 is overpassed. This is the Kaiser effect and can be practically explained by the fact that the damage associated with stress level P1 has occurred during the initial loading cycle and therefore, no extra damage and consequently no AE are indicated in the reloading. With the increase of the load to values higher than P1 (e.g. up to point P2 in the graph), AE starts to be

**Fig. 2** Depiction of the “Kaiser effect” and felicity ratio

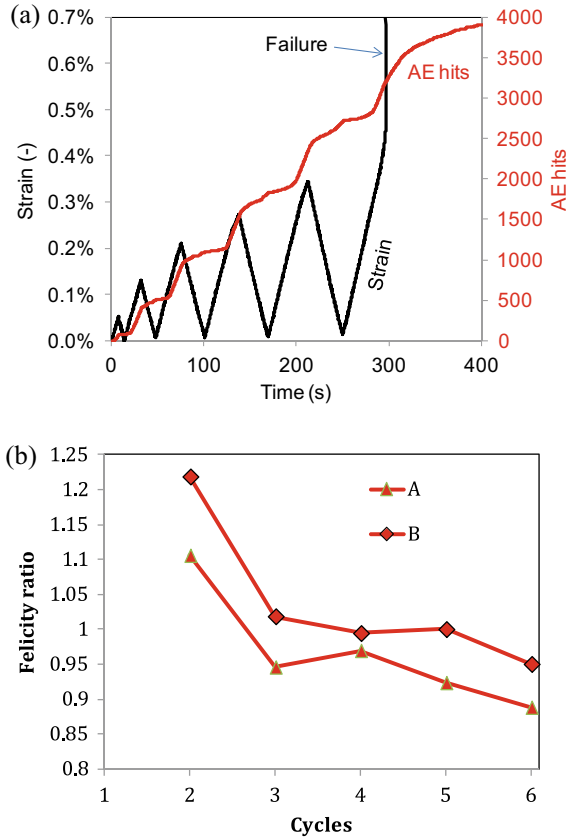


recorded again. Now let us assume that the higher stress level  $P_2$  has caused serious damage in the material. If unloading and reloading takes place again, AE activity will be recorded at lower loads than the previous maximum ( $P_3 < P_2$ ). This can be the result of significant cracks that create stress concentrations and locally increase the stress before the nominal stress reaches the previous maximum level. The ratio of the load at the moment of AE onset, over the previous maximum load (in this case  $P_3/P_2$ ) is defined as “Felicity” ratio (FR) since 1977 when Dr. T. Fowler named the index after his little daughter [5]. When this ratio is close to one (or even higher) it indicates that the Kaiser effect is valid, and the material is intact. Thereafter, the larger the departure of the FR at a value less than unity while cyclic loading continues, the more pronounced the accumulated damage [5–7].

Indicatively, one example is depicted below concerning the cyclic tensile loading of two glass fiber/ceramic matrix coupons (Fig. 3.). In (a) the incremental cyclic strain and cumulative AE histories are depicted, while in (b) the descending behavior of FR is evident. Felicity ratio values higher than 1 are possible as the next crack would require higher load than the previous maximum load (see cycle 2), when the material is still relatively undamaged. A main drop of FR was noticed between the 2nd and 3rd cycle. The specimens failed at the 6th cycle when their FR was about 0.9 [8]. The decreasing trend of FR with load is usually monotonic, however, the exact trend may not always be similar. For example, in [6, 7] FR is reported to decrease linearly with the increase of load for different composites. One should always be cautious about the absolute values and their connection to the structural condition. Although in certain cases like the aforementioned composites in [5–7] a FR of 0.8 or 0.9 was measured just before failure being therefore, connected to heavy damage, there are other cases of materials that the limit is set lower, or even at 0.5 for large concrete structures [9–12].

A global explanation about the origin of the “Felicity” effect is not straightforward. In general, it is discussed in relation to the stresses developed around a damaged area. The stiffness of a fiber-damaged zone is decreased according to the proportion of intact/damaged fibers allowing it to deform more. The stress differentials are then developed on the surrounding intact zone when reloading takes place [7, 13]. On the other hand, the stress differentials induce higher interlaminar stresses leading to premature delaminations in composites. This could be included in the discussion

**Fig. 3** Strain and AE cumulative history (a) and b Felicity ratio for cyclic loading in ceramic composite coupons [8]

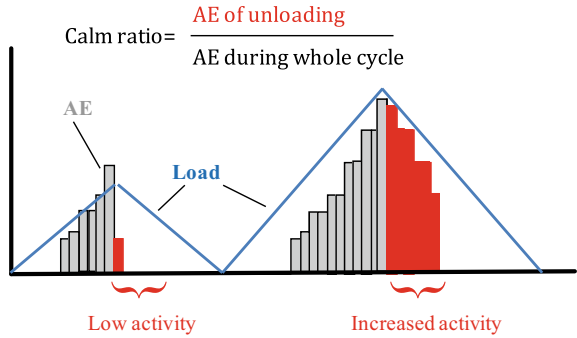


of stress concentration around the tip of a crack. The stresses at the tip are higher compared to the nominal stress. Therefore, at reloading, even at a load lower than the previous maximum, locally the stresses may exceed the strength of the material and induce crack propagation and therefore, AE. In addition, friction between the two sides of an existing crack/delamination is also possible during the reloading step contributing to early AE. High FR (more than 1) even at 90% of the load, imply that fibers remain intact until higher stress levels than older composites showing the advancement of manufacturing of composites as discussed in [6].

Apart from the load, other distress parameters can be used to define Felicity ratio, depending on what is easily measurable. For example, in the case of a train passing on top of a concrete pylon supporting the bridge, the cyclic distress may well be measured by strain gauges on the pylon, since the actual load or stress is difficult to be deduced [11].

On selecting the onset of AE during reloading, one could select the first event or the bending point on the cumulative AE event history [7]. Other deterministic approaches have also been used, like the rate of AE in order to exclude the possibility that the

**Fig. 4** AE in consecutive loading cycles—the activity during unloading increases for higher maximum load



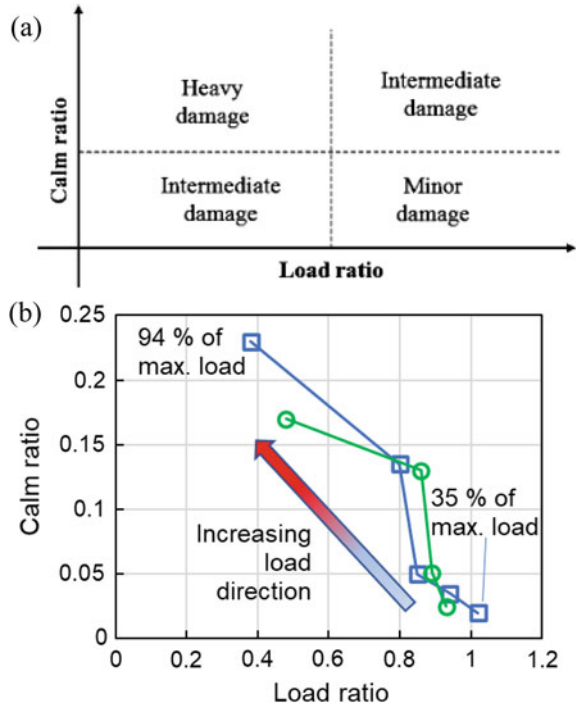
measurement is triggered by one single event, like at least 10 events in 10 s as in [14] or the average of the first 15 events as mentioned in [7].

The aforementioned Felicity ratio parameter is usually combined with the “Calm ratio”. In case of cyclic loading, the activity during the unloading phase is used as another indication of damage. This is quantified by the “Calm ratio” which is defined as the total activity during unloading, over the total activity during the whole cycle (loading and unloading, see Fig. 4) [15], as proposed by the Japanese Society of Non-Destructive Inspection [16].

For structurally stable material, this parameter obtains values close to zero due to limited activity during unloading. However, as damage is accumulated, serious AE is recorded during unloading as well, increasing this ratio even to values higher than 0.5, meaning that the largest part of AE activity may be recorded during the unloading (and not the loading) part of the history. This is a powerful but also an experienced-based index. Simply, the AE activity may come from friction between the crack banks and it increases as the cracks become more and larger. The differentiation between the low and serious damage is defined in combination with other techniques like the visual inspection and may differ according to the conditions. The most important element is the possibly increasing trend of Calm ratio which indicates development of damage. In literature, Calm ratio has been used for evaluation of reinforced concrete beams as well as bridges of pre-stressed concrete [17, 18]. In some examples, the Calm ratio “threshold” between moderate and serious damage is set at 0.5 like in the monitoring of railway piers [11] or even higher in bending of reinforced concrete members [17, 19]. The decrease of the Calm ratio after repair has been used to evaluate the effectiveness of maintenance work in water intake facility (dam) [20]. Calm ratio has also been applied to composites successfully following the damage accumulation after each loading cycle [6, 21].

The combination of the two indices is described in the relevant recommendations [15] and is quite powerful for the evaluation of the material condition. One could mention that the exact threshold between the different regimes (i.e. intact/low/medium/heavy damage) is case-specific but the overall trend shows a monotonic increase of calm ratio and a monotonic decrease of Felicity ratio with additional damage, like the example below. Figure 5a shows the general separation

**Fig. 5 a** Damage characterization on the plane of Calm and Load ratio according to [15], **b** example of characterization from two similar lime hydrate mortar masonry walls under cyclic compression loading [14]



of the plane according to [15], while Fig. 5b, shows a practical example coming from the cyclic compression load of two masonry walls [14]. As the load increases (from 35 to 94%) the calm ratio increases from 0.01 to about 0.2 with a simultaneous decrease of load (Felicity) ratio from 1 to approximately 0.4 [14]. In a recent case in aircraft composite wings under bending, a serious drop in FR as well as increase in the activity during unloading (though not specifically quantified by calm ratio), was used to determine the loading cycle during which serious damage was inflicted [21].

In addition, the intensity analysis can be mentioned. This works again combining two indices: the “Severity Index” and the “Historic Index”. The first is a measure (actually the average) of the magnitude of the 50 strongest AE events for a stage of loading. The latter expresses the changes in the slope of the cumulative signal strength with respect to time and in essence is the ratio of the cumulative signal strength of the recent hits to the cumulative signal strength of all recorded hits up to that moment. The intensity of AE data is obtained by plotting the maximum severity-historic index calculated during each loading phase [22, 23]. This analysis was first developed for FRP tanks but was expanded to other fields like reinforced concrete [24, 25].

The indices discussed above concern the total activity of AE, regardless of the characteristics (e.g. waveform shape, amplitude, frequency etc.). Focusing on specific parameters of the signals, it is reasonable that the amplitude shows correlation to the fracture process. The distribution of amplitude offers valuable information as well.

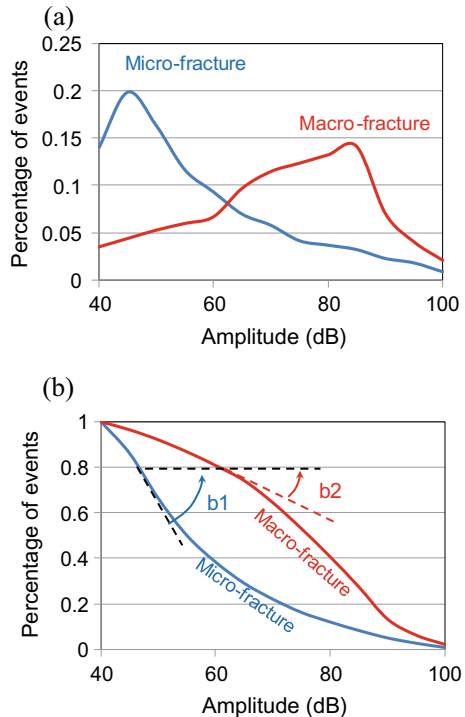


Micro-fracture usually takes place through many small events but macroscopic fracture is expressed by fewer and larger scale events. It is natural therefore, that the statistical event distribution is quite full at the lower end of amplitudes for micro-cracking (e.g. just after 40 dB in the indicative example of Fig. 6a), while macro-fracture exhibits a higher population at higher amplitudes. If we create the cumulative distributions of Fig. 6a, we end up to Fig. 6b. The slope is smaller (in absolute value) for the macro-fracture and this information is quantified through the index b-value or the “improved b-value”, (*ib*-value), which is the slope of the cumulative amplitude distribution of the recent events [26]. The cumulative frequency–magnitude distribution was originally used in seismology to characterize earthquake populations [27, 28]. The formula for the exact calculation is:

$$Ib = \frac{\log_{10} N(\mu - \alpha_1\sigma) - \log_{10} N(\mu + \alpha_2\sigma)}{(\alpha_1 + \alpha_2)\sigma} \tag{3}$$

where  $\mu$  is the average amplitude,  $\sigma$  is the standard deviation and  $\alpha_1$  and  $\alpha_2$  are empirical constants (usually both set to “1”). Finally,  $N(x)$  denotes the part of the population with amplitude higher than  $x$ . Usually a number of 50 or 100 events are calculated in overlapping windows. As seen, the b value is not directly a function of amplitude but of the part of the population above a specific amplitude (e.g. average

**Fig. 6** Amplitude distribution (a) and cumulative distribution (b) of a population of AE events. The b- or the Ib-value express the slope at the amplitude range of interest



plus/minus one standard deviation). Therefore, it does not necessarily indicate higher absolute value of amplitude but basically expresses the ratio between the events of large scale over the events of small scale [29]. This makes it also less sensitive to the attenuation that will anyway interfere with the absolute value of amplitude. Due to the sensitivity of the distribution on the fracture process,  $ib$ -value exhibits serious drops before occurrence of macroscopic damage, in essence acting as warning [26, 29–32].

### 3 Discussion on AE Parameter- and Signal- Based Approaches

Before continuing on more aspects of parameter analysis a brief parenthesis on the mentality of the selected approach follows. Recently some discussion is taking place in the AE community on the “discrimination” between the “parameter based” AE and the “signal based” approach. In fact, both are well documented choices and may well be followed in the same or different applications. The latter mentioned approach is based on recording the whole waveform of each hit. After obtaining the full waveform, a number of options are available given that certain “idealized” assumptions are followed. These concern the point nature of the sensor, or in essence that the active area is much smaller than the wavelength. In addition, that the acquisition system and the material exhibit linear behavior, meaning that the amplitude at the received point is proportional to the amplitude of the source for a constant distance. Using these assumptions, the final waveform recorded through the AE sensor can be described as a convolution between the excitation function (e.g. cracking event), the material’s transfer function, and the response function of the system either in a unified way or having individual functions for the different components i.e. sensor, cables and amplifiers. Given the recorded waveform and the transfer function of the material and system, one can attempt to derive the source function [33, 34]. It enables evaluation of the absolute amplitude or function in general of the received stress waves or the shape of the original wave of the source, provided that the transfer functions of the materials and sensor sensitivity are accurately known. This information can lead to the intensity and time history of the forces acting on the wave source in order to characterize the physical mechanisms which could be either a fracture related event or for example an impact. It also allows sensor calibration and enables comparison of results obtained with different systems, therefore promoting the understanding of the physics of AE, which consequently leads to improved, nondestructive evaluation techniques [34–38]. However, it is understandable that accuracy should be secured for each of the “links” of the chain.

On the other hand, in many applications, it is not necessary to calibrate sensors or to find the exact function of the source in order to solve a certain problem. In addition, the assumptions followed in the previous approach are not always met. For example, in complicated geometries or severely damaged media containing serious heterogeneities, interpretation of full waveforms is not straightforward and may become

unreliable. In those cases, parameter-based approach may work in a simple [39, 40] or more complicated framework (e.g. pattern recognition [2, 41, 42]).

Going back to the signal-based approach one can select to make frequency (FFT) or wavelet analysis [43, 44]. This gives important information on the frequency content as well as the time within the waveform when each frequency band is dominant. A further option is to run MTA (Moment Tensor Analysis) for fracture mode identification [45, 46] in case of homogeneous material provided that at least six sensors record most of the events. This can be very beneficial for many cases of bulk material like concrete where the propagation of waves is three dimensional. As already mentioned, recording the full waveform makes conditionally possible to calculate the transfer function of the material or the exact source function [47]. More details are given to the corresponding Chap. [Signal-Based AE Analysis](#) of this book about signal-based AE analysis. However, the waveforms may have a length of thousands of points, selected by the user. Having full waveforms requires more recording space. Although this may not cause serious limitations in regular conditions nowadays, it may result in huge file sizes in case of fatigue experiments and in situ. Also, at moments of high emission rate (e.g. main fracture of fibrous composites) it may compromise the recording rate for multiple channels, as a certain time window is needed for the storage of the data, during which no new waveform is recorded. Therefore, in different cases the users may select not to record the full waveforms. In fact, the early AE boards developed decades ago did not have the capacity of digitizing a full waveform. Therefore, measurement and recording of some basic parameters (feature extraction) was the next best option. This is a way to compress the information keeping of course some indicative parameters with strong characterization power over the phenomena under investigation. Instead of maintaining thousands of points corresponding to a full waveform, the basic information is maintained by a few parameters like the amplitude, the duration, the rise time, the average frequency etc. This way, a waveform of thousands of points is reduced to a “vector” of approximately twenty to thirty basic parameters. Although this is literally an effective way to compress data, at the same time some information is lost and there is no chance to make elaborate analysis (e.g. to distinguish between different wave modes within the waveform in case of Lamb waves).

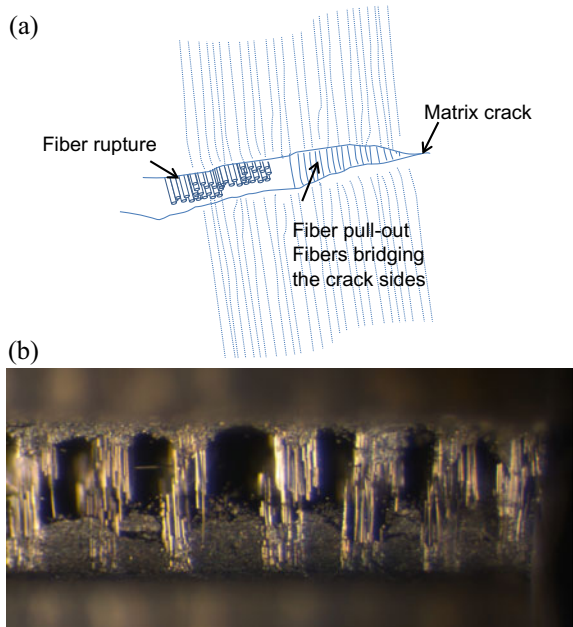
Nowadays, contemporary AE equipment can record full waveforms. Therefore, it is the choice of the user whether to analyze full waveforms or analyze directly their parameters. In reality, these options should be seen as complementary approaches and not as different or even contradicting ones. In many cases, simultaneous use of both approaches led to similar classification results [48, 49], showing that both can be used to treat the problem at hand. As an example, in [48] the shear events during bending of a reinforced concrete beam, were calculated at 55% of the total population using MTA and at 51% using simple classification based on AF and RA parameters.

## 4 Fracture Mode Evaluation Through AE Parameters

In this subsection, the use of AE parameters, also called “signal descriptors” in several cases [2, 42], for characterization of the fracture mode is discussed. This book contains specialized chapters concerning different material fields so the examples can be considered as indicative but not exhaustive for each material, focusing on the application of parameter-based analysis. The fracture mode is of paramount importance for the structural behavior of components. In most of the cases, structural materials are fibrous (e.g. aeronautics, automotive) or particulate composites (concrete, metal alloys), they bear reinforcing bars or patches. Due to their complexity, their fracture includes different mechanisms. One typical example in the field of composite materials is the initial cracking of the matrix which usually starts at low load, while at higher load, phenomena like fiber debonding and pull-out, delaminations and fiber rupture are exhibited, as indicatively seen in Fig. 7. An illustration closer to civil engineering is shown in Fig. 8. The cases on the left include shearing action meaning that the sides of the cracks move in parallel but at opposing directions (due to the external patch, internal reinforcement or shear stresses in the matrix). On the right side, there is the simple tensile case like a normal crack due to bending.

Since shear phenomena separate the reinforcement from the weaker matrix, they are considered crucial for the mechanical performance. It is generally accepted that these phenomena occur at high load levels and lead to final fracture, while the tensile phenomena are observed in low load while the structural integrity has not yet been

**Fig. 7** **a** Geometric representation of the fracture mechanisms in fibrous composites, **b** microphotograph of carbon fibers rupture and debonding in ceramic matrix composite. Some fibers are ruptured but the main part of the bundle is just pulled out of the matrix [8]



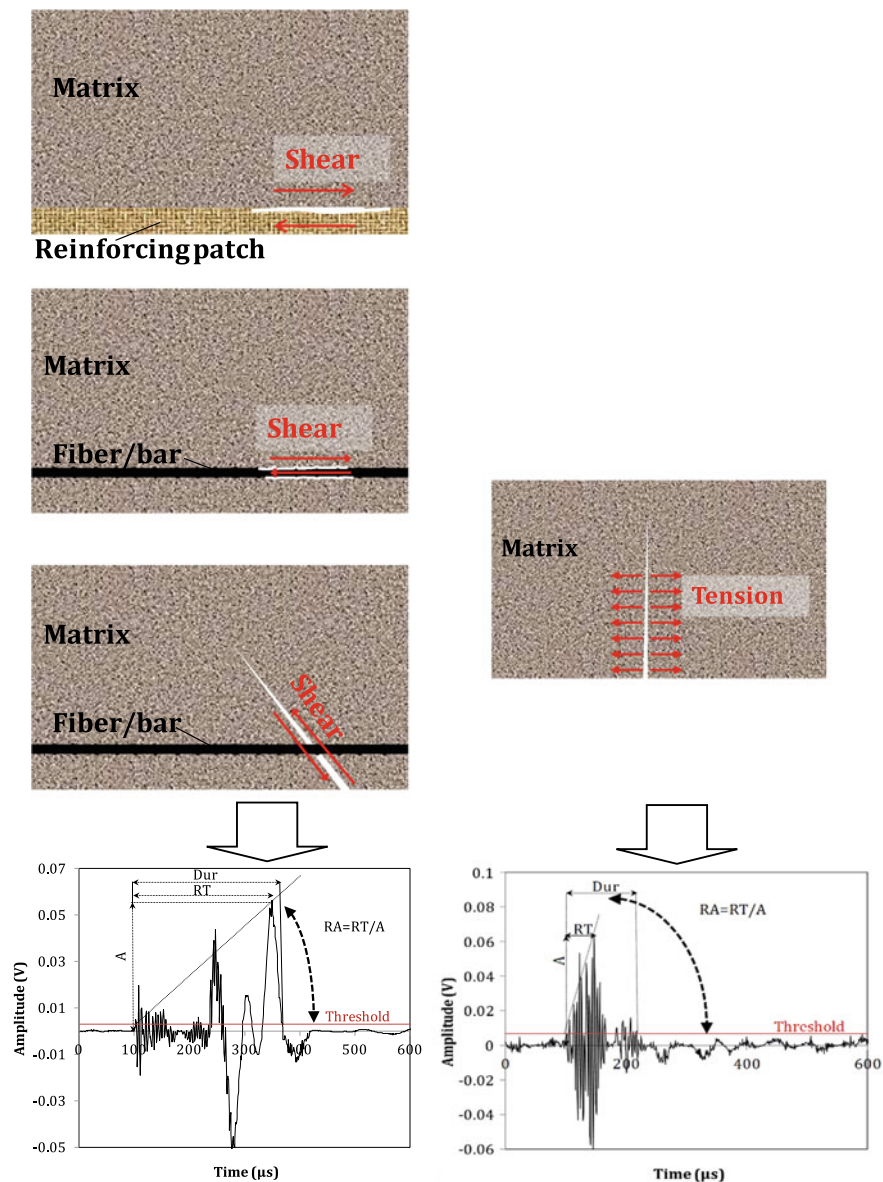


Fig. 8 Fracture modes and relevant AE waveforms

compromised. In this respect, the characterization of the fracture mode supplies important information for structural integrity [15]. This can be part of a whole Structural Health Monitoring (SHM) process of a structure or a study of mechanical behavior in laboratory conditions.

It has been well supported in AE literature that the fracture mode plays an important role on the emitted signal's characteristics. For example, during fracture in fiber composites, the rupture of a fiber bundle is expected with high speed due to the stiffness of the fiber material and relatively small propagation length (close to one fiber/bundle diameter) [50]. On the other hand, if fiber/matrix debonding occurs, the situation will alter: the propagation speed will be lower and the damage propagation step is expected longer as the crack will come to a rest only when stopped by other filaments or after long distance of propagation until the stress is released. It is reasonable therefore, to expect increased bandwidth towards the higher frequency bands for fiber rupture and longer duration characteristics for shear debonding [50].

Apart from the original bandwidth of the source, an important parameter is the proportion of the different wave modes triggered by the source. Tensile events emit higher frequencies and shorter waveforms. Due to the higher proportion of longitudinal waves over the shear, most of the energy arrives early within the waveform and results in shorter duration and rise time. Therefore, parameters like AF and PF obtain higher values in comparison to shear events. In contrast, parameters like DUR, RT, RA are higher for shear events, because the major part of the AE energy goes into the formation of shear waves which are slower and arrive later than the initial longitudinal arrivals. Figure 9 shows a simple illustration for the cases of tensile and shear strains on a "representative volume element". Tensile strain induces a volumetric change in the material and if a crack occurs, the energy is released in the longitudinal wave mode. On the contrary, shear stresses induce a shape change which is typical of shear waves. This has been verified with Boundary Element Method simulations, dealing with a surface opening crack on a bulk material, where the shear excitation clearly produced longer waveforms as received by an AE sensor on the surface. Furthermore, this was more pronounced as the distance from the source increased due to the differential velocity of the separate wave modes (in this case longitudinal, shear and Rayleigh), see Fig. 10 [50].

In plate structures, instead of the bulk waves, the situation is transformed into a Lamb wave problem, with cracks vertical to the length of the plate emitting their energy mostly in the fast symmetric mode (S0), while cracks parallel to the sides (could be delaminations in layered media) excite the slower antisymmetric (A0). Depending therefore, on the type of the damage propagation event, the waveform shape, and therefore, its parameters will change: delamination events with stronger A0 mode are expected with longer RT, duration and lower frequency indicators [52, 53]. It is easily understandable that with so wide length scale and loading patterns in all types of materials the above discussed effects obtain a stochastic character [50]. However, the basic concept that different fracture modes induce different frequency content and other waveform characteristics like RT, DUR in general has been supported by simulations and experiments in different types of materials such as composites, concrete, masonry [50, 54–66].

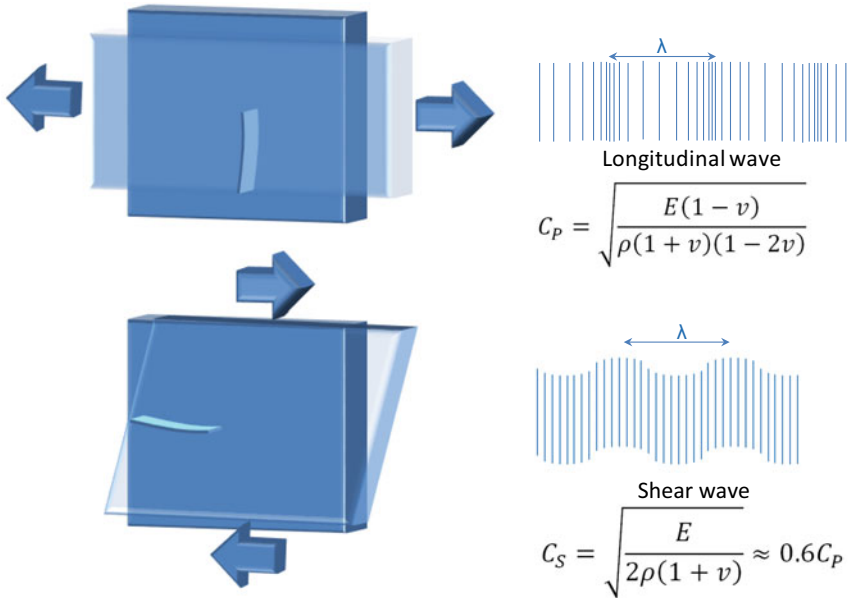


**Fig. 9** Deformations due to tensile (top) and shear (bottom) forces, related excited wave mode after cracking and corresponding velocities

Looking in more detail in composites, as aforementioned, it is widely accepted that the four basic damage mechanisms are distinguishable by their AE signature, namely: matrix cracking, fiber/matrix debonding, delaminations and fiber rupture. A trend commonly accepted is that delaminations are characterized by longer waveforms, matrix cracks and debonding events by medium durations and fiber rupture by very short rise times and durations [55]. Apart from shape parameters (e.g. aforementioned duration and rise time), parameters related to frequency and amplitude have been successfully applied. In [67] RMS (root means squared) amplitude was used to distinguish between failure mechanisms in CFRP aeronautic plates (delaminations, matrix cracking and fiber breakage) after adequate filtering. In [68, 69] the amplitude distribution enhanced with principal components analysis were used to analyze AE data from fracture of cross-ply and 3D woven glass/epoxy specimens under tension.

An overview of related literature is given in [55, 68], where expected amplitude and frequency distributions are summarized for different composite material systems and testing setups (mainly sensor sensitivities). Considering the same sensor type, fiber rupture led to higher amplitude distributions than matrix cracking while delaminations and pull-out was in between. In some cases, the distributions overlap not allowing an absolute determination of the exact mechanism based on the amplitude like in [68, 70] but in others the amplitude is a parameter able solely to characterize the damage mechanism, as in [71, 72]. Similar is the situation for frequency which shows higher range of values for fiber rupture and lower for matrix cracking. Indicatively, as measured by broadband sensors in tensile specimens with Glass or Carbon fibers

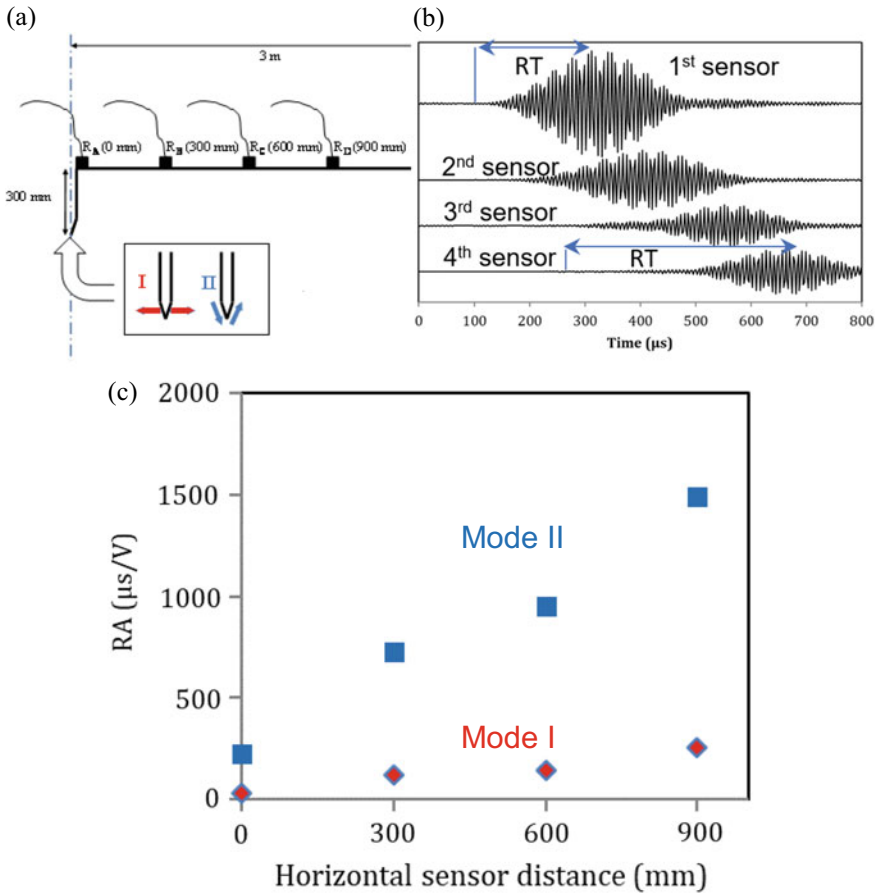


**Fig. 10** a Surface breaking crack under mode I or mode II displacement in a stiff bulk medium, b simulated waveforms of the four sensors of (a), c RA calculated from the simulated waveforms [51]

[73–75] fiber breakage showed frequency higher than 300 or 500 kHz while matrix cracks around 100 kHz with fiber debonding being in the middle (200–300 kHz). In [76] along other analyses that takes place with the full waveform (short time Fourier transformation), peak frequencies are used to distinguish between fiber breakage (600 kHz) and friction between fibers (200 kHz) in ceramic fiber mat. In any case, it should be noted that the same source mechanism, e.g. crack growth, may release different amount of energy in different materials or under different stress conditions. Furthermore, propagation conditions (i.e. attenuation) have a further effect on the acquired waveform. Therefore, no simple correspondence between measured AE amplitude, energy or frequency and damage mechanism should be taken for granted before validation. It would certainly be simplistic to use previously developed classification rules for a new experiment without considering the differences in material,



sensor type and source location. As also mentioned previously, a high frequency source of fiber rupture would lose much of its frequency content while propagating to a remote transducer through a heterogeneous composite starting to resemble a (low frequency anyway) signal from debonding or matrix crack which occurred close to the sensor. However, these relative trends among different mechanisms are quite well founded through numerous experiments in different laboratories as already discussed earlier in the chapter.

For cases where proper results cannot be obtained with simple schemes, pattern recognition approaches based on AE parameters have been successfully applied in composites as in [2, 68, 69, 77–80] while a more comprehensive historical review related to pattern recognition can be found in the work of Ono and Gallego [7].

A simple but powerful scheme for crack classification has been extensively used and is prescribed in relevant recommendations for concrete [1]. It concerns the relation between two time-domain parameters, namely the AF and RA which have already been introduced. The RA value is calculated in units of time over waveform amplitude (ms/V or  $\mu$ s/V) and the population of signals is drawn in the plane of AF and RA (see Fig. 11). If the amplitude is given in logarithmic scale (dB) it should be transformed in voltage (do not forget that due to piezoelectric phenomenon the sensors produce electric waveform.)

The amplitude A is expressed:

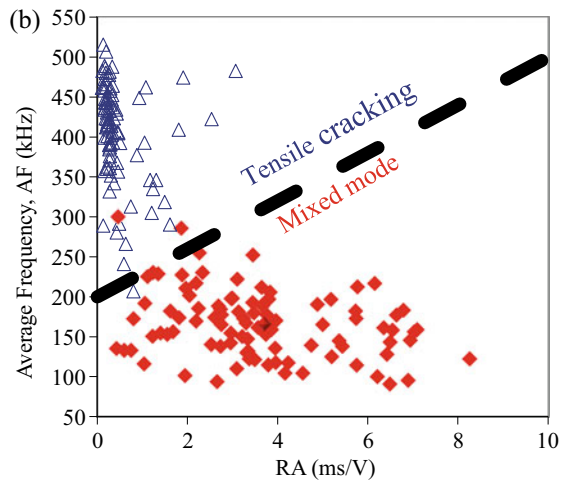
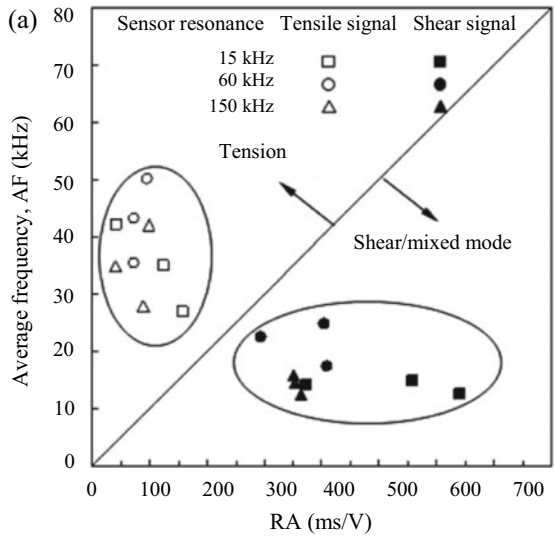
$$A(dB) = 20 \cdot \log\left(\frac{V}{V_{ref}}\right) - G \quad (4)$$

where G is the gain of the pre-amplifier and  $V_{ref}$  the reference voltage (usually 1  $\mu$ V). The above equation is solved for V and obtains units of Volts.

In cases of laboratory experiments the populations of tensile and other signals can be well distinguished even with a single diagonal line, with the top left part belonging to tension and the lower-right belonging to shear/mixed mode as can be seen indicatively in [39, 40, 48, 61, 62], see example of Fig. 11b. In any case the separation line is not constant and depends on the conditions of the experiment (geometry, sensor type and distances). As aforementioned, attenuation plays a very important role decreasing the amplitude and frequency content while possibly increasing the duration of waveform at least up to a distance. This way, the results have a certain dependence on the position of sensors relatively to the sources [31, 42, 50, 51, 78, 79, 81, 82]. This influence that is evident in the waveform and its parameters, is transferred through the whole characterization analysis lowering the success of the classification [78, 83], therefore, the expansion to large scale is not straightforward. This is treated in more detail in the chapter dedicated to plate waves.

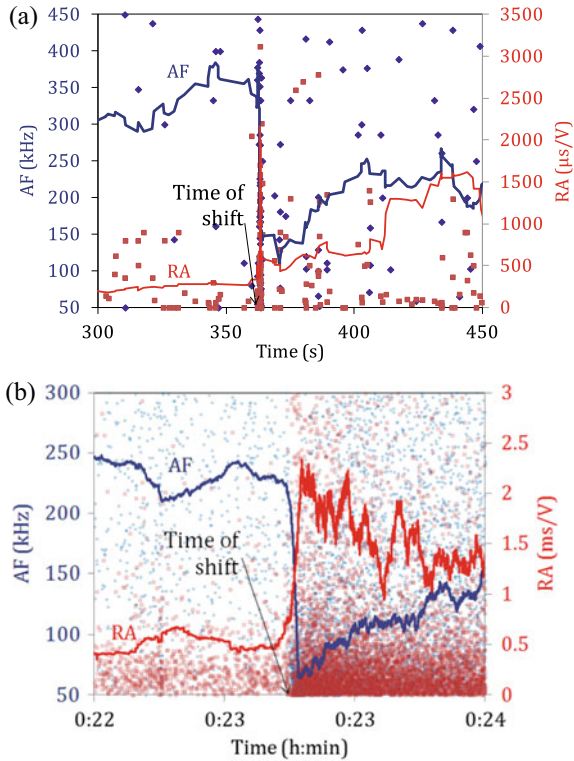
In any case, if the absolute classification would be desired, the separation line (tensile/shear) should be defined from the start for any different type of experiment. However, in most of the applications the shift of the parameters is already indicative of the transition between different fracture modes and an absolute separation has no special meaning considering the difficulties to produce an accurate result. Figure 12 concerns steel fiber reinforced concrete during bending from [59]. Apart from the

**Fig. 11** Classification of AE signals based on the fracture mode of concrete with **a** resonant sensors [1], **b** broadband sensors (in SFRC) [39]



points that correspond to AF and RA, the moving average trend line of the recent 50 hits is also presented. Until 350 s the average line of AF is fluctuating between 300–400 kHz that correspond to the micro-cracking of the cementitious matrix due to the tensile stress at the bottom. At the moment of the macroscopic fracture (at approximately 360 s), apart from the cracking, another dominant failure mechanism is activated. This is the pull-out for the fibers that are bridging the crack sides which of course resembles shear. This causes a strong drop of frequency content (AF drops to approximately 150 kHz). Correspondingly, until the moment of macro-fracture, the RA line fluctuated around 200  $\mu$ s/V, while at the moment of failure it reached several thousands and never returned to values below 500  $\mu$ s/V. These changes take place in

**Fig. 12** Use of AF and RA for monitoring the fracture of **a** steel fiber reinforced concrete beams under bending [59], **b** textile reinforced cement beams under bending [60]



less than one second and signify the shift between the two fracture mechanisms and the process from the first stage of crack formation to the stage of crack widening.

The next example of Fig. 12b concerns a glass fiber cementitious composite coupon. In this case as well, the increase of RA (from 0.5 to 2 ms/V) and decrease of AF (from 230 to 70 kHz) signify the onset of delaminations between successive plies and fiber pull-out events, while just a few seconds before, the dominant mechanism was the micro-cracking due to bending load [60].

In [84], concretes with nanoSiO<sub>2</sub> exhibited higher RA value compared to reference concrete mix. According to the authors this is related to the fact that nanoparticles act as ultra-fine aggregates and become obstacles to crack propagation. As another example of characterization with AE parameters, AE MARSE Energy in correlation to the plastic strain energy of reinforced concrete beams under bending indicated the moment of reinforcement yield: after this moment most of the mechanical energy was consumed in yield of the reinforcement which, however, does not emit much AE due to ductility [85]. In [86] AE energy is correlated with the energy dissipation from different mechanisms, like matrix cracking and fiber pull-out in ultra-high-performance concrete during cylinder splitting test. In [87], a masonry bridge was analyzed based on the number of events and their energy, which pinpointed the localized sources corresponding to an actual crack in the structure. Several studies

on AE waveform parameters as well as Felicity, Calm ratio and b-value can be found in the review papers [23, 88].

Passing to some indicative examples of parameter analysis in the field of metals, the superior time resolution of AE (in the order of  $\mu\text{s}$ ) is increasingly recognized as a means to study microstructural deformations [89]. In [89] the characteristic peaks of count rates close to the tensile yield point were attributed to a synergetic effect of twin nucleation and massive dislocation motion in pure Mg and Mg–Al alloy specimens under uniaxial testing. Efforts have been done to correlate AE amplitude distribution and frequency indices (PF and CF) with the level of strain sustained by Aluminum specimens [90]. AE population (classified events and total hits) were well correlated to the fatigue cycles in steel material simulating a gear box [91]. In the same study signal analysis takes place based on the power spectrum, separating the “continuous” AE due to plastic deformation of steel (main band 100–150 kHz) from crack propagation events that showed main content at higher bands. On a similar approach in additively manufactured titanium, the RT was used to characterize signals related to crack propagation during fatigue in bending, while the localized events rate followed quite well the progressively increasing load levels [92]. In fatigue experiments of CT aluminum specimens, RA value, measured by relatively broadband sensors with center at 450 kHz, sharply increased about 1000 cycles before final failure, indicating the shift of the fracture mode from tension to shear, which accelerated the crack propagation rate [93]. Steel specimens of similar shape but larger dimensions were tested in fatigue in [94] with simultaneous monitoring by five AE sensors resonant at 150 kHz. In this case, the crack propagation rate and the stress intensity factor were correlated with the AE absolute energy and the counts leading to a prognosis methodology concerning the critical point when fatigue cracks become unstable. In [95] the RA value exhibited its highest activity when the steel specimens reached their yield point under monotonic tensile loading. Two types of sensors (resonant at 150 and 75 kHz) were simultaneously used providing, as expected, different values, but the same trends. In another study, AE parameters obtained up to 60% of the maximum stress were used in an Artificial Neural Network approach to predict the final strength of Al/SiC particulate composites under tension. Specifically, the authors used RA, amplitude distribution and Felicity ratio predicting the strength with an error of approximately 3% [96]. Interesting results from metal matrix composites were reported in [97] where aluminum alloys were reinforced with different volume percentage and different size of SiC particles and tested under four-point bending. Monitoring took place with two AE sensors of 180 kHz resonant frequency. It was shown that in the case of unreinforced specimens and reinforced with 1  $\mu\text{m}$  particles, AE was negligible in terms of total events and of low amplitude (less than 70 dB), while for the case of larger SiC particles of 20  $\mu\text{m}$ , AE events were approximately 50 times more and with amplitudes reaching 90 dB. This was attributed to the fact that void nucleation at bigger particles caused both the number and the amplitude of the events to be higher. This difference between particle size was much more pronounced in AE than the particle volume content, where 10 or 30% did not show similarly striking differences.

Parameter analysis is also widely used for practical applications related to SHM of structures. A reason is that huge amount of redundant data is not easy to handle or store in field conditions. Therefore, practitioners prefer the compressed information of the AE parameters, rather than treating full lengthy waveforms. In [98] high temperature thick-walled structures were monitored during cooling down. The cooling process establishes a thermal gradient and thus thermal strains, which allows for detecting of possible active flaws. Several AE parameters like amplitude, energy, severity and historic index were used to characterize sources while an automated grading system for the sources was established. A recent study [99] describes the application of wireless AE for active corrosion monitoring in a decommissioned reactor facility with resonant and broadband sensors. Monitoring of such installations is of particular interest due to safety concerns, while the reinforced concrete used for their construction is prone to several degradation processes, like reinforcement corrosion, freeze-thaw, alkali-silica reaction etc. The authors used parameter-based filters to reject non meaningful data and validated that areas with observable damage yielded much more AE activities with higher amplitude. The high levels of activity indicated that damage in the form of corrosion and related cracking was progressing. Contour plots of CSS (Cumulative Signal Strength or another term for absolute energy) are presented showing the areas with higher damage and being validated by the AE sources in 2D localization. In addition, CSS curves followed well the accelerated corrosion process in a block extracted from the facility, showing three distinct stages: high rate at the start of corrosion process, then a dormant period with less activity followed by an increase in rate being in accordance with the electrochemical readings at that location. Several applications are described in [100] concerning pipelines, roller bearings of rotary kilns and dragline metal excavator machine. For example, in the case of the excavator, higher count rate was monitored upon excavating or loading the bucket when it is more likely that cracks can grow and during unloading of the bucket when crack sides may rub each other. In contrast rotating of the excavator did not produce significant emissions. In the same paper concerning a metal highway bridge an interesting observation comes, that meaningful signals propagating longer than 7 m start to resemble noise signals in terms of average frequency (designated as counts/duration) and energy, while signals originating up to 2 m away from the sensor can be clearly distinguished. In [101] AE monitoring in a movable stadium roof truss revealed correlation between the displacement rate and the peak amplitude of AE, showing sensitivity to the “stick-slip” behavior of the mechanism. The displacement during slip is small, however, it occurs instantaneously resulting in sudden energy release. As a last indicative example, the AE from cable rupture in 10 m long prestressed concrete beams was distinguished from friction between the cable and the grout based primarily on their AF: cable rupture resulted in frequencies above 50 kHz as measured by 60 kHz resonant sensors [102].

## 5 Conclusions

Parameters are a form of compressed information extracted by the AE waveforms. This chapter summarizes indicative application of AE parameters for material condition monitoring. Basic definitions are given concerning pure waveform descriptors as well as indices based on AE activity. Their use towards evaluation of structural condition is discussed and different examples are shown to illustrate their characterization power in various material fields. As aforementioned, the above examples are just indicative of the vast number of applications of AE parameter analysis in materials research and (SHM). In these and many other cases in literature it is obvious that analysis of AE parameters yields unique information for the succession of the fracture mechanisms in a material, bringing the advantage of simplicity. It must be highlighted however, that much effort is still necessary in the field of recommendations in order to promote a unified system of characterization while relevant efforts are unfolding [15].

## References

1. Ohtsu M (2010) Recommendations of RILEM Technical Committee 212-ACD: acoustic emission and related NDE techniques for crack detection and damage evaluation in concrete: test method for classification of active cracks in concrete structures by acoustic emission. *Mater Struct* 43(9):1187–1189
2. Philippidis TP, Nikolaidis VN, Anastassopoulos AA (1998) Damage characterization of carbon/carbon laminates using neural network techniques on AE signals. *NDT & E Int* 31(5):329–340
3. Shiotani T (2006) Evaluation of long-term stability for rock slope by means of acoustic emission technique. *NDT & E Int* 39:217–228
4. Kaiser J (1950) Untersuchung über das Auftreten von Geräuschen beim Zugversuch. PhD Thesis, Technische Hochschule Munich
5. Fowler TJ (1977) Acoustic emission testing of fiber reinforced plastics. ASCE Fall Convention, San Francisco
6. Waller JM, Saulsbury RL, Andrade E (2010) Use of acoustic emission to monitor progressive damage accumulation in Kevlar 49 composites. In: QNDE conference, vol 29, AIP Conf. 1211, pp 1111–1118
7. Ono Kanji, Gallego Antolino (2012) Research and applications of AE on advanced composites. *J Acoust Emission* 30:180–229
8. Aggelis DG, Dassios KG, Kordatos EZ, Matikas TE (2013) Damage accumulation in cyclically-loaded glass-ceramic matrix composites monitored by acoustic emission. *Sci World J*
9. Alander P, Lassila LV, Tezvergil A, Vallittu PK (2004) Acoustic emission analysis of fiber-reinforced composite in flexural testing. *Dent Mater* 20(4):305–312
10. Kocur GK, Vogel T (2010) Classification of the damage condition of preloaded reinforced concrete slabs using parameter-based acoustic emission analysis. *Construct Build Mater* 24:2332–2338
11. Luo Xiu, Haya Hiroshi, Inaba Tomoaki, Shiotani Tomoki (2006) Seismic diagnosis of railway substructures by using secondary acoustic emission. *Soil Dyn Earthquake Eng* 26:1101–1110
12. Liu Z, Ziehl P (2009) Evaluation of reinforced concrete beam specimens with acoustic emission and cyclic load test methods. *ACI Struct J* 106(3):288–299

13. Hamstad MA (1986) A discussion of the basic understanding of the Felicity effect in fiber composites. *J Acoustic Emission* 5:95–102
14. Shetty N, Livitsanos G, Van Roy N, Aggelis DG, Van Hemelrijck D, Wevers M, Verstryngne E (2019) Quantification of progressive structural integrity loss in masonry with Acoustic Emission-based damage classification. *Constr Build Mater* 194:192–204
15. Ohtsu M (2010) Recommendation of RILEM TC 212-ACD: acoustic emission and related NDE techniques for crack detection and damage evaluation in concrete. Test method for damage qualification of reinforced concrete beams by acoustic emission. *Mater Struct* 43(9):1183–1186
16. NDIS 2421 (2000) Recommended practice for in situ monitoring of concrete structures by acoustic emission. Japanese Society for Non-Destructive Inspection
17. Ohtsu M, Uchida M, Okamoto T, Yuyama S (2002) Damage assessment of reinforced concrete beams qualified by acoustic emission. *ACI Struct J* 99(4):411–417
18. Aggelis DG, Shiotani T, Terazawa M (2010) Assessment of construction joint effect in full-scale concrete beams by acoustic emission activity. *J Eng Mech* 136(7):906–912
19. Colombo S, Forde MC, Main IG, Shigeishi M (2005) Predicting the ultimate bending capacity of concrete beams from the “relaxation ratio” analysis of AE signals. *Constr Build Mater* 19:746–754
20. Shiotani T, Aggelis DG (2007) Evaluation of repair effect for deteriorated concrete piers of intake dam using AE activity. *J Acoustic Emission* 25:69–79
21. Esola S, Wisner BJ, Vanniamparambil PA, Geriguis J, Kotsos A (2018) Part qualification methodology for composite aircraft components using acoustic emission monitoring. *Appl Sci* 8:1490
22. El Batanouny MK, Ziehl PH, Larosche A, Mangual J, Matta F, Nanni A (2014) Acoustic emission monitoring for assessment of prestressed concrete beams. *Construct Build Mater* 58:46–53
23. Behnia A, Chai HK, Shiotani T (2014) Advanced structural health monitoring of concrete structures with the aid of acoustic emission. *Construct Build Mater* 65:282–302
24. Fowler TJ, Blessing JA, Conlisk PJ (1989) New directions in testing. In: *Proceedings of the 3rd international symposium on AE from composite materials*. Paris, France
25. Golaski L, Gebiski P, Ono K (2002) Diagnostics of reinforced concrete bridges by acoustic emission. *J Acoustic Emission* 20:83–98
26. Shiotani T, Fujii K, Aoki T, Amou K (1994) Evaluation of progressive failure using AE sources and improved B-value on slope model tests. *Progress Acoustic Emission* 7:529–534
27. Hainzl S, Fischer T (2002) Indications for a successively triggered rupture growth underlying the 2000 earthquake swarm in Vogtland/NW Bohemia. *J Geophys Res* 107(B12):2338
28. Gutenberg B, Richter C (1954) *Seismicity of the earth and associated phenomena*. Princeton University Press, Princeton, NJ, USA
29. Kurz JH, Finck F, Grosse CU, Reinhardt HW (2006) Stress drop and stress redistribution in concrete quantified over time by the B-value analysis. *Struct Health Monitor* 5:69–81
30. Carnì DL, Scuro C, Lamonaca F, RS Olivito, Grimaldi D (2017) Damage analysis of concrete structures by means of acoustic emissions technique. *Compos B* 115:79–86
31. Vidya Sagar R, Rao MVMS (2014) An experimental study on loading rate effect on acoustic emission based b-values related to reinforced concrete fracture. *Construct Build Mater* 70:460–472
32. Aggelis DG, Soulioti DV, Sapouridis N, Barkoula NM, Paipetis AS, Matikas TE (2011) Acoustic emission characterization of the fracture process in fibre reinforced concrete. *Constr Build Mater* 25(11):4126–4131
33. Eitzen DG, Wadley HNG (1984) Acoustic emission: establishing the fundamentals. *J Res Natl Bureau Stand* 89(1)
34. Prosser WH (2002) Acoustic emission (Ch. 6). In: Shull PJ (ed) *Nondestructive evaluation, theory, techniques and applications*. Marcel Dekker, New York, pp 369–446
35. McLaskey GC, Glaser SD (2012) Acoustic emission sensor calibration for absolute source measurements. *J Nondestruct Eval* 1–12

36. Ohtsu M, Ono K (1986) The generalized theory and source representation of acoustic emission. *J Acoust Emission* 5:124–133
37. Green ER (1998) Acoustic emission in composite laminates. *J Nondestruct Eval* 17(3):117–127
38. Sause MGR, Horn S (2010) Simulation of acoustic emission in planar carbon fiber reinforced plastic specimens. *J Nondestruct Eval* 29(2):123–142
39. Aggelis DG (2011) Classification of cracking mode in concrete by acoustic emission parameters. *Mech Res Commun* 38:153–157
40. Shahidan S, Pulin R, Muhamad Bunnori N, Holford KM (2013) Damage classification in reinforced concrete beam by acoustic emission signal analysis. *Constr Build Mater* 45:78–86
41. Pandya DH, Upadhyay SH, Harsha SP (2013) Fault diagnosis of rolling element bearing with intrinsic mode function of acoustic emission data using APF-KNN. *Expert Syst Appl* 40(10):4137–4145
42. Godin N, Reynaud P, Fantozzi G (2018) Challenges and limitations in the identification of acoustic emission signature of damage mechanisms in composites materials. *Appl Sci* 8:1267
43. Baccar D, Söffker D (2015) Wear detection by means of wavelet-based acoustic emission analysis. *Mech Syst Signal Process* 60:198–207
44. Zitto ME, Piotrkowski R, Gallego A, Sagasta F, Benavent-Climent A (2015) Damage assessed by wavelet scale bands and b-value in dynamical tests of a reinforced concrete slab monitored with acoustic emission. *Mech Syst Signal Process* 60:75–89
45. Ohtsu M, Okamoto T, Yuyama S (1998) Moment tensor analysis of acoustic emission for cracking mechanisms in concrete. *ACI Struct J* 95(2):87–95
46. Grosse C, Reinhardt H, Dahm T (1997) Localization and classification of fracture types in concrete with quantitative acoustic emission measurement techniques. *NDT E Int* 30(4):223–230
47. Grosse CU, Linzer LM (2008) Ch. 5 signal-based AE analysis. In: Grosse CU, Ohtsu M (eds) *Acoustic emission testing*, pp 53–99
48. Ohno K, Ohtsu M (2010) Crack classification in concrete based on acoustic emission. *Construct Build Mater* 24(12):2339–2346
49. Kawasaki Y, Wakuda T, Kobara T, Ohtsu M (2013) Corrosion mechanisms in reinforced concrete by acoustic emission. *Constr Build Mater* 48:1240–1247
50. Sause M, Hamstad M (2018) Acoustic emission analysis. In: Beaumont PWR, Zweben CH (eds) *Comprehensive composite materials II*, vol 7. Academic Press, Oxford, pp 291–326
51. Polyzos D, Papacharalampopoulos A, Shiotani T, Aggelis DG (2011) Dependence of AE parameters on the propagation distance. *J Acoustic Emission* 29:57–67. [www.ndt.net/article/jae/papers/29-057.pdf](http://www.ndt.net/article/jae/papers/29-057.pdf)
52. Eaton M, May M, Featherston C, Holford KM, Hallet S, Pullin R (2011) Characterisation of damage in composite structures using acoustic emission. *J Phys: Conf Ser* 305:012086
53. Gresil M, Saleh MN, Soutis C (2016) Transverse crack detection in 3D angle interlock glass fibre composites using acoustic emission. *Mater* 9:699
54. Li L, Lomov SV, Yan X (2015) Correlation of acoustic emission with optically observed damage in a glass/epoxy woven laminate under tensile loading. *Compos Struct* 123:45–53. <https://doi.org/10.1016/j.compstruct.2014.12.029>
55. Chandarana N, Sanchez DM, Soutis C, Gresil M (2017) Early damage detection in composites during fabrication and mechanical testing. *Materials* 10:685
56. Sause MGR, Haider F, Horn S (2009) Quantification of metallic coating failure on carbon fiber reinforced plastics using acoustic emission. *Surf Coat Technol* 204:300–308. <https://doi.org/10.1016/j.surfcoat.2009.07.027>
57. Bohse J (2004) Acoustic emission examination of polymer-matrix composites. *J Acoustic Emission* 22:208–223. [www.ndt.net/article/jae/papers/22-208.pdf](http://www.ndt.net/article/jae/papers/22-208.pdf)
58. Kourkoulis SK, Dakanali I (2017) Pre-failure indicators detected by acoustic emission: Alfás stone, cement-mortar and cement-paste specimens under 3-point bending. *Frattura ed Integrità Strutturale* 40:74–84



59. Aggelis DG, Soulioti DV, Gatselou EA, Barkoula N-M, Matikas TE (2013) Monitoring of the mechanical behavior of concrete with chemically treated steel fibers by acoustic emission. *Constr Build Mater* 48:1255–1260
60. Blom J, El Kadi M, Wastiels J, Aggelis DG (2014) Bending fracture of textile reinforced cement laminates monitored by acoustic emission: influence of aspect ratio. *Constr Build Mater* 70:370–378
61. Elfergani HA, Pullin R, Holford KM (2013) Damage assessment of corrosion in prestressed concrete by acoustic emission. *Constr Build Mater* 40:925–933
62. Livitsanos G, Shetty N, Hündgen D, Verstryngne E, Wevers M, Van Hemelrijck D, Aggelis DG (2018) Acoustic emission characteristics of fracture modes in masonry materials. *Constr Build Mater* 162:914–922
63. Saidane EH, Scida D, Assarar M, Ayad R (2017) Damage mechanisms assessment of hybrid flax-glass fibre composites using acoustic emission. *Compos Struct* 174:1–11
64. Masmoudi S, El Mahi A, Turki S (2015) Use of piezoelectric as acoustic emission sensor for in situ monitoring of composite structures. *Compos B Eng* 80:307–20
65. Gutkin R, Green C, Vangrattanachai S, Pinho S, Robinson P, Curtis P (2011) On acoustic emission for failure investigation in CFRP: pattern recognition and peak frequency analyses. *Mech Syst Signal Process* 25(4):1393–407
66. Kolanu NR, Raju G, Ramji M (2019) Damage assessment studies in CFRP composite laminate with cut-out subjected to in-plane shear loading. *Compos B Eng* 166:257–271
67. Martínez-Jequier J, Gallego A, Suárez E, Juanes FJ, Valea Á (2015) Real-time damage mechanisms assessment in CFRP samples via acoustic emission Lamb wave modal analysis. *Compos B Eng* 68:317–326
68. Li L, Lomov V, Yan X, Carvelli V (2014) Cluster analysis of acoustic emission signals for 2D and 3D woven glass/epoxy composites. *Compos Struct* 116:286–299
69. Godin N, Huguet S, Gaertner R (2005) Integration of the Kohonen's self-organising map and k-means algorithm for the segmentation of the AE data collected during tensile tests on cross-ply composites. *NDT E Int* 38:299–309
70. Masmoudi S, El Mahi A, Turki S, El Guerjouma R (2014) Mechanical behavior and health monitoring by acoustic emission of unidirectional and cross-ply laminates integrated by piezoelectric implant. *Appl Acoust* 86:118–125
71. Liu PF, Chu JK, Liu YL, Zheng JY (2012) A study on the failure mechanisms of carbon fiber/epoxy composite laminates using acoustic emission. *Mater Des* 37:228–235
72. Mahdavi HR, Rahimi GH, Farrokhabadi A (2015) Failure analysis of ( $\pm 55$ )<sub>9</sub> filament-wound GRE pipes using acoustic emission technique. *Eng Fail Anal* 62:178–187
73. Ramirez-Jimenez CR, Papadakis N, Reynolds N, Gan TH, Purnell P, Pharaoh M (2004) Identification of failure modes in glass/polypropylene composites by means of the primary frequency content of the acoustic emission event. *Compos Sci Technol* 64:1819–1827
74. De Groot PJ, Wijnen PAM, Janssen RBF (1995) Real-time frequency determination of acoustic emission for different fracture mechanisms in carbon/epoxy composites. *Compos Sci Technol* 55:405–41
75. Nikbakht M, Yousefi J, Hosseini-Toudeshky H, Minak G (2017) Delamination evaluation of composite laminates with different interface fiber orientations using acoustic emission features and micro visualization. *Compos B Eng* 113:185–196
76. Ito K, Enoki M (2007) Acquisition and analysis of continuous acoustic emission waveform for classification of damage sources in ceramic fiber mat. *Mater Trans* 48(6):1221–1226
77. Anastassopoulos AA, Philippidis TP (1995) Clustering methodology for the evaluation of acoustic emission from composites. *J Acoustic Emission* 13:11–22
78. Farhidzadeh A, Mpalaskas A, Matikas TE, Farhidzadeh H, Aggelis DG (2014) Fracture mode identification in cementitious materials using supervised pattern recognition of acoustic emission features. *Construct Build Mater* 67:129–138
79. Farhidzadeh A, Salamone S, Singla P (2013) A probabilistic approach for damage identification and crack mode classification in reinforced concrete structures. *J Intell Mater Syst Struct* 24(14):1722–1735

80. Brunner AJ (2018) Identification of damage mechanisms in fiber-reinforced polymer-matrix composites with acoustic emission and the challenge of assessing structural integrity and service-life. *Construct Build Mater* 173:629–637
81. Aggelis DG, Mpalaskas AC, Ntalakas D, Matikas TE (2012) Effect of wave distortion on acoustic emission characterization of cementitious materials. *Construct Build Mater* 35:183–190
82. Aggelis DG, Tsangouri E, Van Hemelrijck D, Meccanica (2015) Influence of propagation distance on cracking and debonding acoustic emissions in externally reinforced concrete beams 50:1167–1175
83. Aggelis DG, El Kadi M, Tysmans T, Blom J (2017) Effect of propagation distance on acoustic emission fracture mode classification in textile reinforced cement. *Construct Build Mater* 152:872–879
84. Nazerigivi A, Nejati HR, Ghazvinian A, Najigivi A (2018) Effects of SiO<sub>2</sub> nanoparticles dispersion on concrete fracture toughness. *Construct Build Mater* 171:672–679
85. Sagasta F, Benavent-Climent A, Roldán A, Gallego A (2016) Correlation of plastic strain energy and acoustic emission energy in reinforced concrete structures. *Appl Sci* 6:84
86. Landis EN, Kravchuk R, Loshkov D (2019) Experimental investigations of internal energy dissipation during fracture of fiber-reinforced ultra-high-performance concrete. *Front Struct Civ Eng* 13(1):190–200
87. Shigeishi M, Colombo S, Broughton KJ, Rutledge H, Batchelor AJ, Forde MC (2001) Acoustic emission to assess and monitor the integrity of bridges. *Construct Build Mater* 15(1):35–49
88. Vidya Sagar R, Raghu Prasad BK (2012) A review of recent developments in parametric based acoustic emission techniques applied to concrete structures. *Nondestruct Test Eval* 27(1):47–68
89. Vinogradov A, Máthis K (2016) Acoustic emission as a tool for exploring deformation mechanisms in magnesium and its alloys in situ. *JOM* 68(12):3057–3062
90. Zhang L, Oskoe SK, Li H, Ozevin D (2018) Combined damage index to detect plastic deformation in metals using acoustic emission and nonlinear ultrasonics. *Materials* 11:2151
91. Zhang L, Ozevin D, Hardman W, Timmons A (2017) Acoustic emission signatures of fatigue damage in idealized bevel gear spline for localized sensing. *Metals* 7:242
92. Strantzà M, Van Hemelrijck D, Guillaume P, Aggelis DG (2017) Acoustic emission monitoring of crack propagation in additively manufactured and conventional titanium components. *Mech Res Commun* 84:8–13
93. Aggelis DG, Kordatos EZ, Matikas TE (2011) Acoustic emission for fatigue damage characterization in metal plates. *Mech Res Commun* 38(2):106–110
94. Jianguo Y, Ziehl P, Zárate B, Caicedo J (2011) Prediction of fatigue crack growth in steel bridge components using acoustic emission. *J Construct Steel Res* 67(8):1254–1260
95. Lyasota I, Kozub B, Gawlik J (2019) Identification of the tensile damage of degraded carbon steel and ferritic alloy-steel by acoustic emission with in situ microscopic investigations. *Arch Civil Mech Eng* 19(1):274–285
96. Mahil Loo Christopher C, Sasikumar T, Suresh S (2019) Detection of crack development with Al/SiCp using tensile with online acoustic emission. *J Alloys Compounds* 778:951–961
97. Rabiei A, Kim B-N, Enoki M, Kishi T (1997) A new method based on simultaneous acoustic emission and in-situ SEM observation to evaluate the fracture behavior of metal matrix composites. *Scripta Materialia* 37(6):801–808
98. Papasalouros D, Bollas K, Kourousis D, Anastasopoulos A (2016) Acoustic emission monitoring of high temperature process vessels & reactors during cool down. In: *Emerging technologies in non-destructive testing VI—proceedings of the 6th international conference on emerging technologies in nondestructive testing*. ETNDT 2016, pp 197–201
99. Abdelrahman M, ElBatanouny M, Dixon K, Serrato M, Ziehl P (2018) Remote monitoring and evaluation of damage at a decommissioned nuclear facility using acoustic emission. *Appl Sci* 8:1663
100. Elizarov SV, Barat VA, Terentyev DA, Kostenko PP, Bardakov VV, Alyakritsky AL, Koltsov VG, Trofimov PN (2018) Acoustic emission monitoring of industrial facilities under static and cyclic loading. *Appl Sci* 8:1228

101. Kosnik DE (2016) Review of acoustic emission source mechanisms on large movable structures. In: Shiotani T, Wakayama S, Enoki M, Yuyama S (eds) *Progress in acoustic emission XVIII*. pp 447–455
102. Shiotani T, Oshima Y, Goto M, Momoki S (2013) Temporal and spatial evaluation of grout failure process with PC cable breakage by means of acoustic emission. *Construct Build Mater* 48:1286–1292